A Simplified Contact Model for Sandy Grains Cemented with Methane Hydrate

Un modèle simplifié pour les contacts entre grains de sable cimentés par hydrates de méthane

Jiang M., Liu F., Zhu F., Xiao Y.
Department of Geotechnical Engineering, Tongji University, Shanghai 200092, China
Key Laboratory of Geotechnical and Underground Engineering (Tongji University), Ministry of Education, Shanghai 200092, China

ABSTRACT: Methane hydrates (MHs), regarded as one of the most promising future energies, extensively occupy the voids of soil deposits in permafrost regions and deep seabed. The presence of MH largely changes the macro-mechanical properties of the host deposits due to MH bonds among soils particles. This study introduces a new contact model for soil grains cemented by MH. This model was experimentally calibrated from two rods cemented by different materials. The bond failure criterion was then related to the strength properties of MH considering the effects of temperature, confining pressure, density and saturation of MH. The new model was implemented into a discrete element code to simulate the mechanical response of a MH bearing soil specimen subjected to biaxial loading conditions. The comparison between the simulation and experimental results shows that the new contact model can qualitatively capture the effects of MH cementation. Strain softening and shear dilation of soils cemented with MH become remarkable due to the presence of MH bonds. The cohesion of the MH bearing deposit substantially increases with the hydrate saturation, while the internal friction angle is less affected.

RÉSUMÉ : Les hydrates de méthane (MH) sont considérés comme une source énergétique potentielle fondamentale pour le futur. Ils abondent dans les régions avec permafrost et sur les fonds marins profondes. Les MH influencent grandement les propretés macro-mécaniques des sols qui les contiennent en raison de liens qu'ils forment entre les particules des sols granulaires. Dans ce papier, on introduit un nouveau modèle pour les liens entre particules de sol cémentes par MH. Le modèle a été calibré utilisant des données expérimentales de pairs de barres métalliques (barres de Schneebeli) cimentées par diffèrent matériaux. Le critère de rupture pour les liens (bonds) a été corrélé aux paramètres de résistance au cisaillement des MH incluant les effets de la température, la pression de confinement, la densité et la saturation des MH. Le modèle a été implémenté dans un logiciel aux éléments discrets pour simuler la réponse mécanique des échantillons de sols contenant des MH chargés en conditions biaxiales. La comparaison entre les résultats expérimentaux et numériques montre que le nouveau modèle reproduit qualitativement les effets de la cimentation des liens MH. On a observé que les liens MH causent un adoucissement et dilatation remarquables. La cohésion et l'angle de frottement des sols contenant MH augmentent avec le dégrée de saturation des hydrates avec une augmentation plus significative pour la cohésion que pour l'angle de frottement.

KEYWORDS: Methane hydrate bearing sands; bond; contact model; distinct element method; granular material

1 INTRODUCTION

As promissing resource of future energy, methane hydrates (MHs) are extensively found in voids of sediments situating in seabeds and permafrost regions at low temperatures and high pressures (e.g., Kvenvolden, 1988). They greatly enhances the strength of the host sediments. Moreover, MHs are prone to dissociation due to change in envrionmental conditions and human activities (e.g., installation offshore infrasturcutes). Serious geohazards such as marine landslides are likely triggered by instability of methane hydrate bearing sediments (MHBS). Unfortunately, the mechanism of these geo-hazards is poorly understood due to the lack of robust constitutive model of MHBS in addition to limited experimental data.

A variety of influencing factors on mechanical properties of MHBS were investigated using special triaxial compression aparatus (Hyodo et al. 2005; Masui et al. 2005). In particular, the hydrate habit (i.e., the distribution of MHs in the pore scale) strongly affects properties of MHBS. For example, hydrates acting as inter-particle cementation cause larger strength and stiffness than pore-filling hydrates. It implies that hydrate habit should be featured in a robust constitutive model. However most models derived from laboratory tests at the macro scale are unable to build the connection between macroscopic properties of MHBS and micro structure of hydrate at the pore scale.

In the contrast, the distinct element model (DEM) proposed by Cundall and Strack (1979) provides a solution for simulating hydrate habits at the grain scale. Waite et al., (2009) identified three habits: (1) pore filling with hydrates nucleating in the pore without bridging two or more soil grains together; (2) load bearing with hydrate bridging nearby soil grains and taking part in the strong force chains of the granular assembly; and (3) cementation with hydrates cementing at inter-particle contacts as illustrated in Fig. 1(a). The first type naturally turns into the second when the hydrate saturation exceeds 25-40%. Pore-filling hydrate has been successfully modeled by Brugada et al. (2010) and Jung et al. (2012) using DEM. However the model of cementation-type hydrate remains unsolved partially due to the difficulty in quantifying the strength of MH bonds. This constitutes the strong motivation of this paper. The objective of this study is to develop a suitable bond contact model for MHBS, which is of critical importance to produce meaningful macro-mechanical response of MHBS via DEM.

2 A BOND CONTACT MODEL FOR MHBS

2.1 *A conceptual bond contact model and laboratory data*

Fig. 1 shows a conceptual bond contact model (Jiang et al. 2006) of two disks with radii R_1 and R_2 bonded at a finite width B and a central thickness t. A dimensionless parameter β is defined in terms of common radius $\overline{R}=2R_1R_2/(R_1+R_2)$:

$$\beta = B/\overline{R} \tag{1}$$

Figs. 1(b) to (d) illustrate how this model responds to the normal contact force F_n, the shear contact force F_s, and the contact moment M. These contact forces can be computed as:

$$F_n = \min[K_n u_n, R_{nb}] \quad (2a)$$

$$F_s = \min[K_s u_s, R_{sb}] \quad (2b)$$

$$M = \min[K_m \theta, R_{rb}] \quad (2c)$$

where min[•] is the operator taking the minimum value; u_n, u_s and θ are the overlap, relative shear displacement, and relative rotation angle; K_n, K_s and $K_m = K_n \beta \bar{R}/12$ are the normal, tangential and rolling contact stiffness; R_{nb}, R_{sb}, and R_{rb} are the normal, shear and rolling bond strength.

For simplicity, the inter-particle rolling resistance is ignored at contacts with broken bonds or without bonds. At these contacts, the linear contact law applies:

$$F_n = K'_n u_n \quad (3a)$$

$$F_s = \min[K'_s u_s, \mu F_n] \quad (3b)$$

where μ is the inter-particle friction coefficient; K'_n and K'_s are the post-failure normal and tangential contact stiffness.

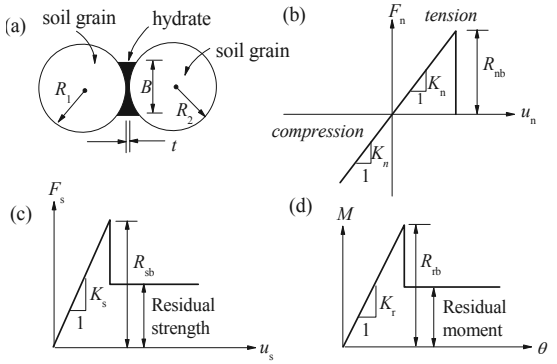

Figure 1. Schematic illustration of (a) MH bonded soil grains and its response: (b) F_s against u_n; (c) F_s against u_s; and (d) M against θ

Jiang et al. (2012a, 2012b) performed microscopic contact mechanical test to calibrate the model parameters for a large number of aluminous rod pairs (with a diameter of 12 mm and a length of 50 mm) bonded by epoxy and cement. Their study resulted in a generic criterion for bond failure, forming a strength envelope in a three-dimensional space with axes being F_n, F_s, and M. The projection of the envelope in F_s-M plane can be approximated as an ellipse as the following:

$$\frac{F_s^2}{R_{sb}^2} + \frac{M^2}{R_{rb}^2} = 1 \quad (4)$$

The ellipse varies in size with increasing F_n. That is, R_{sb} and R_{rb} are functions of F_n. For the case of thick bonds, they can be computed as follows based on experimental findings if only normal forces are applied on the bond:

$$R_{sb} = f_s \cdot L_s \cdot (F_n + R_t) \cdot [(R_c - F_n)/(F_n + R_t)]^n \quad (5a)$$

$$R_{rb} = f_r \cdot L_r \cdot (F_n + R_t) \cdot [(R_c - F_n)/(F_n + R_t)]^m \quad (5b)$$

where R_t and R_c are the bond tension and compression strength, respectively, which can be obtained from tension/compression test of the cementation materials. L_s and L_r are the slopes of the straight line linking R_t to the peak shear strength or peak rolling resistance on the projection plane. f_s, f_r, n and m are fitting parameters to the experimental data. They can be calibrated from contact mechanical tests as Jiang et al. (2012a, 2012b) did recently. Fig. 2 illustrates their test results with a comparison to the prediction by Eq. (5).

Since MH remains stable in very extreme conditions, it is still a challenge to directly measure the strength parameters for hydrate bonds. Thus, in addition to test data from similar bond materials, assumptions are necessary for indirectly determining model parameters for MH bonds. This will be explained later.

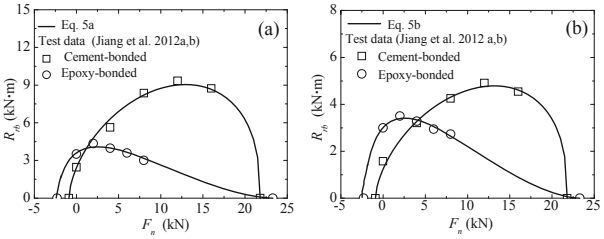

Figure 2. Bond strength envelopes derived from laboratory data: (a) strength envelope for R_{sb}; and (b) strength envelope for R_{rb}

2.2 *Determing β from hydrate saturation*

The parameter β relates to a given value of hydrate saturation S_H, which is defined in a two-dimensional context as the ratio of the area of voids occupied by MH, A_H, to the total void area, A_V. The area of voids occupied by the i^{th} MH bond is:

$$A_{bi} = \bar{R}_i^2 \left[2\beta - \beta\sqrt{1 - \frac{\beta^2}{4}} - 2\arcsin\left(\frac{\beta}{2}\right) \right] \quad (6)$$

where we assume (1) the radii of the two bonded particles equal to $\bar{R}_i$ (i.e. neglecting the different curvatures of the particles); and (2) the bond thickness is negligibly small. The total area occupied by hydrate bonds, A_b, can be found by summation over all the bonds. Saturation attributed to pore-filling and bonding hydrates are denoted as S_{Hb} and S_{Hp}, respectively. S_{Hp}, generally equal to 20-30% (Masui et al. 2005), can be regarded as the threshold value of hydrate saturation at which MHs start to bond sand grains. Accordingly,

$$S_H = S_{Hb} + S_{Hp} = \frac{A_H}{A_V} = (1 + e_p)\frac{A_b}{A} + S_{Hp} = \frac{(1 + e_p)}{A}\sum_{i=1}^{m} A_{bi} + S_{Hp} \quad (7)$$

where m is the total number of bonds; A is the total area of a cross section of the sample; e_p is the planar void ratio. Eq. (7) provides a non-linear relationship which depends on the state of compaction of the sample (e.g. relative density) which rules the particle packing and therefore the value of m. Fig. 3(a) shows a sample curve achieved for the case of a dense soil sample (e.g., e_p= 0.21) consisting particles with diameters ranging from 6 to 9 mm forming a gradation curve as shown in Fig. 3(b).

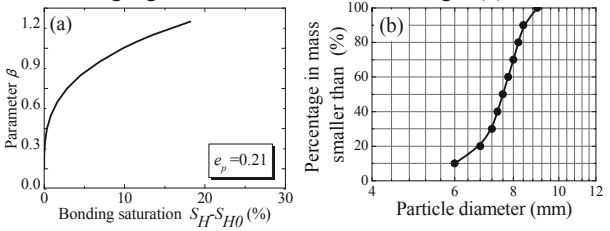

Figure 3. (a) Model parameter β at different hydrate saturation for a dense sample (e_p=0.21) with (b) a given gradation curve

2.3 *Contact stiffness*

Soil grains with the Young's modulus ranging from 50 to 70 GPa can be regarded as rigid particles relative to MH. Thus, for MH-bonded grains, $K_n = BE/t$. The Young's modulus of MH, E, depends on temperature T, confining pressure p_c and density ρ according to the test data (Hyodo et al. 2005). The regression analysis of these data yields the empirical formula:

$$E/p_a = 3(p_c/p_a) + 4950.50(\rho/\rho_w) - 1.98(T/T_0) - 1821.78 \quad (8)$$

where p_a is standard atmospheric pressure (i.e., 0.1 MPa); ρ_w is the water density at 4˚C; T_0 is the reference temperture (1˚C is used herein).

The tangential contact stiffness K_s then relates to K_n based on PFC2D Guidelines (Itasca, 2004) by $K_s = 2/3\ K_n$.

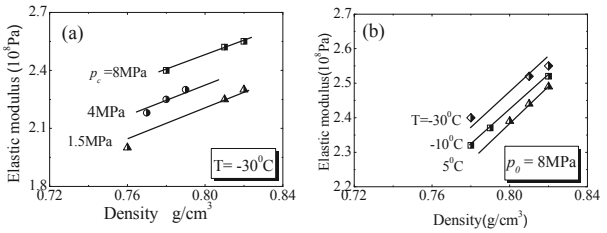

Figure 4. Elastic modulus of pure MH measured (a) at a given temperature but varied confining pressure; and (b) at a given confining pressure but varied temperatures (data from Hyodo et al. 2005)

2.4 *Bond tension/compression strength*

The bond tension and compression strength (i.e., R_t and R_c in Eqs. (4) and (5)) can be computed from the tension/compression strength, $q_{max,t}$ and $q_{max,c}$, of pure MH specimen subjected to a given confining pressure p_c, i.e.,

$$R_t = \beta \bar{R} q_{\max,t} \tag{9a}$$

$$R_c = \beta \bar{R} q_{\max,c} \tag{9b}$$

As partially shown in Fig. 5, the peak deviator stress $q_{max,c}$ obtained from the compression triaxial test on pure MH specimens is a function of T, p_c and ρ (Hyodo et al. 2005). The regression analysis of these data yields another empirical formula:

$$q_{\max,c}/p_a = 0.81(p_c/p_a) - 2.08(T/T_0) + 184.16(\rho/\rho_w) - 134.65 \tag{10a}$$

Eq. (9) is assumed to hold for tension triaxial test as well, leading to the following:

$$q_{\max,t}/p_a = 0.81p' - 2.08(T/T_0) + 184.16(\rho/\rho_w) - 134.65 \tag{10b}$$

where

$$p' = 0.55(p_c/p_a) + 1.15(T/T_0) - 100.09(\rho/\rho_w) + 74.39 \tag{11}$$

2.5 *Fitting parameters*

As already demonstrated in Fig. 2, the shape of the bond strength envelope is controlled by the cementation materials, resulting in different values of fitting parameters used in Eqs. (4) and (5). Direct calibration of those parameters are rather difficult for hydrate bonds. We assume that bond strengths are dominated by the strength properties of cementation materials. Fig. 6(a) shows the yielding curves of different materials. The yielding curve is left skewed for cement-based materials and right skewed for epoxy. Unfortunately, we are not able to present the yielding curve for MH due to insufficiency of test data available. As an ice-like material, MH was found similar to ice in some physical properties (Solan et al. 1998; Dvorkin et al. 2000) and mechanical properties (Nabeshima et al. 2003; Choi et al. 2009). Instead of MH, the yielding curve of ice is plotted in Fig. 6(b) for comparison, which displays left skewed. We concluded that the MH bonds produce a bond strength envelope similar to cement bonds. The fitting parameters calibrated using cement-bonded grains are used for MH-bonded grains. Eq. (5) is re-written as:

$$R_{sb} = 1.16 \cdot 0.498 \cdot (F_n + R_t) \cdot [(R_c - F_n)/(F_n + R_t)]^{0.38} \tag{12a}$$

$$R_{rb} = 1.13 \cdot 0.96 \cdot (F_n + R_t) \cdot [(R_c - F_n)/(F_n + R_t)]^{0.38} \tag{12b}$$

Suppose a MHBS sample collected at 800 m below the sea level (giving a pore water pressure of 8 MPa applied on MH bonds in the sample) at 5˚C. The gradation curve of the soil grains is assumed to be Fig. 3(b) and the initial void ratio of the sample is 0.21. For a given S_{Hb}, the parameter β is determined from the chart presented in Fig. 3(a). R_t and R_c computed from Eqs. (9) to (11) are then substituted into Eq. (12) to obtain the bond strength envelope. Fig. 7 illustrates a series of strength envelopes at different levels of hydrate saturation. As expected, the envelope expands omothetically with S_{Hb}.

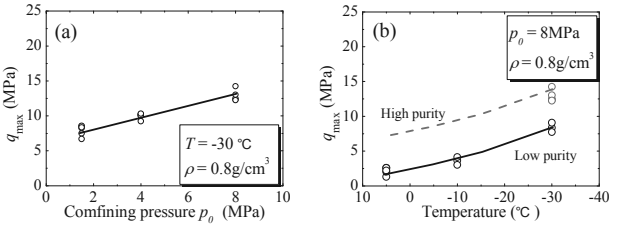

Figure 5. The maximum deviator stress of pure MH measured (a) at a given temperature but varied confining pressure; and (b) at a given confining pressure but varied temperatures (data from Hyodo et al. 2005)

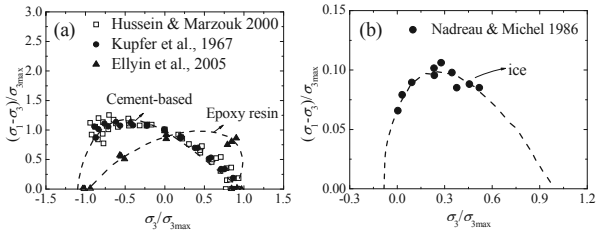

Figure 6. Yielding curves obtained from experiments for: (a) cement-based materials and epoxy resin; and (2) ice

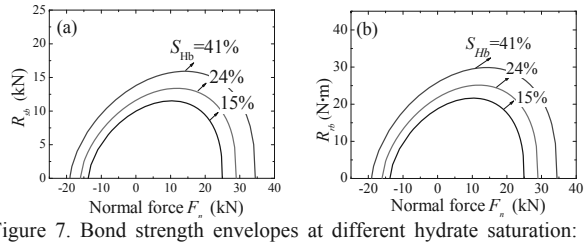

Figure 7. Bond strength envelopes at different hydrate saturation: (a) relationship between R_{sb} and F_n; and (b) relationship between R_{rb} and F_n

3 DEM SIMULATION OF BIAXIAL TESTS ON MHBS

The proposed model for MHBS was implemented into the commercial code PFC2D for simulating the biaxial compression test on a MHBS specimen. For inter-particle contacts with broken bonds or without bonds, $\mu = 0.5$, $K'_n = 3.0\times10^8$ N/m, $K'_s = 2.0\times10^8$ N/m. The model parameters for other contacts with intact MH bonds were determined as explained in Section 2.

A 40×80 cm virtual specimen was first generated using the multi-layer with under-compaction method (Jiang et al. 2003). The resulted specimen with an initial planar void ratio of 0.21 was composed of 6000 disks with radii ranging from 6 to 9 mm, forming a gradation curve shown in Fig. 3(b). The specimen was consolidated by applying an isotropic pressure of 1 MPa until force balance was maintained. The gravity was ignored in the whole simulation. Bonds were then assigned to the contacts of particles. As the force system was balanced, the top wall moved downward at a speed of 5% per minute to simulate the displacement-controlled shearing process. Frictionless rigid walls were used in the simulation in stead of flexible walls to reduce the computational time. The boundary type selected will not affect the stress-strain response, while it however will change the formation of shear bands.

4 SIMULATION RESULTS

The simulation was conducted on four specimens at S_{Hb} = 0%, 15%, 24% and 41% at a pore water pressure of 8 MPa and a temperature of 5˚C in order to compare to the experimental data published in Masui et al. (2005). S_{Hp} is assumed to be approximately 26% according to the data in Masui et al. (2005).

Fig. 8 shows the simulated stress-strain response at an effective confining pressure of 1 MPa and test results obtained under the same conditions. Although the simulation can not quantitatively reproduce the tests, it captures the essential features such as strain softening at S_H > 26%. At higher S_H, the peak strength is mobilized when the axial strain exceeds approximately 3%, and the residual strength coincides at a large strain regardless of hydrate saturation due to complete breakage of hydrate bonds. This agrees well with experimental data. However the peak deviator stress obtained from the simulation is lower than the test results. Besides the difference between biaxial and triaxial tests, one of the reasons is that the bond tension and compression strength could be underestimated in the model. The size of the specimen used in material strength tests is much larger than inter-particle bonds in MHBS. The strength measured from a large specimen is much lower than that of a much smaller specimen.

Fig. 9(a) presents an example of the stress-strain behavior under different confining pressures, which leads to a relationship between the peak strength parameters and S_H as depicted in Fig. 9(b). The presence of hydrate cause the increase in cohesion, while no significant change in the internal friction angle is found associated with increasing S_H. This agrees well with the experimental observation (Masui et al. 2005). However the friction angle obtained from the simulation (approximately 20˚) is lower than the test data (approximately 30˚). This could be improved by introducing the inter-particle rolling resistance in the model. The micro parameters associated with the rolling resistance can be first calibrated from a simulation on a specimen without MH bonds in order to reach high friction angle. These parameters set are then brought into MHBS model. Considering the inter-particle rolling resistance will result in a higher peak deviator stress, which better matches the test data as shown in Fig. 8(b).

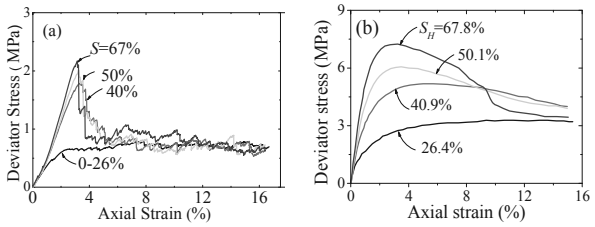

Figure 8. Deviator stress vs. axial strain: (a) DEM simulation; and (b) triaxial test results performed by Masui et al. (2005)

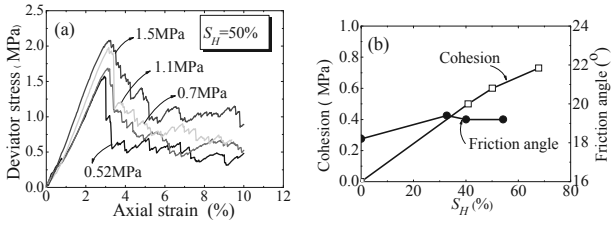

Figure 9. Simulation result (a) deviator stress vs. axial strain at different confining pressure for a specimen with SH=50%; and (b) peak strength parameters at different SH.

5 CONCLUSIONS

This paper proposed a two-dimensional bond contact model of MHBS for considering the bonding effect of MH. The bond strength envelope was partially derived from laboratory data. The model parameters are related to the hydrate saturation, confining pressure, temperature and density of MH. Using this model, the DEM simulation of the biaxial test is capable of capturing the major mechanical response of MHBS specimen such as strain softening and shear dilation at high hydrate saturation. This study can help to better understand the connection of the microscopic formation habit of MH to macroscopic mechanical behaviors of MHBS.

Though the DEM simulation produced results qualitatively comparable to available test data, quantitative agreement remains still a challenge. The current model ignores the bond thickness, which however affects the hydrate saturation and the bond strength parameters. Consideration of inter-particle rolling resistance in the model will improve the model performance. Moreover, the size effect on the bond strength remains unclear and deserves more caution. Further investigation on these issues is definitely needed in the future work.

ACKNOWLEDGEMENTS

This work is funded by China National Funds for Distinguished Young Scientists (No. 51025932), and the EU FP7 IRSES grant (No. 294976).

REFERENCES

Brugada J. et al. 2010. Discrete element modelling of geomechanical behaviour of methane hydrate soils with pore-filling hydrate distribution. *Granular Matter* 12(5, SI): 517-525.

Cundall P.A. and Strack O.D.L. 1979. A discrete numerical model for granular assemblies. *Géotechnique* 29(1), 47–65.

Ellyin F. and Xia Z.H. 2006. Nonlinear viscoelastic constitutive model for thermoset polymers. *Journal of Engineering Materials and Technology* 128:579-585.

Hussein A. and Marzouk H. 2000. Behavior of high-strength concrete under biaxial stresses. *ACI Materials Journal* 97(1):27-36.

Hyodo M. et al. 2005. Basic research on the mechanical bahavior of methane hydrate-sediments mixture. *Japanese Geotechnical Society* 45(1):75-85.

Jiang M.J. et al. 2003. An efficient technique for generating homogeneous specimens for DEM studies. *Computers and Geotechnics* 30(7): 579-597.

Jiang M.J. et al. 2012a. Contact behavior of idealized granules bonded in two different interparticle distances: An experimental investigation. *Mechanics of Materials* 55: 1-15.

Jiang M.J. et al. 2012b. An experimental investigation on the mechanical behavior between cemented granule, *Geotechnical Testing Journal* (*ASTM*) 35(5): 678-690.

Jiang M.J. et al. 2006. Bond rolling resistance and its effect on yielding of bonded granulates by DEM analyses. *International Journal for Numerical and Analytical Methods in Geomechanics* 30(8): 723-761.

Jung J. et al. 2012. Stress-strain response of hydrate-bearing sands: Numerical study using discrete element method simulations. Journal of Geophysical Research-Solid Earth, 117, B04202, doi:10.1029/2011JB009040.

Kupfer H. et al. 1969. Behavior of concrete under biaxial repeated loading. *ACI Journal Proceedings* 66(52): 656-666.

Kvenvolden K.A. 1988. Methane hydrate-a major reservoir of carbon in the shallow geosphere? *Chemical Geology* 71(1-3):41-51.

Masui A. et al. 2005. Effects of methane hydrate formation on shear strength of synthetic methane hydrate sediments. *Proceedings of the 5th International Offshore and Polar Engineering Conference*, Seoul, Korea: 364-369.

Nadreau J.P. and Michel B. 1986. Yield and failure envelope for ice under multiaxial compressive stresses. *Cold Regions Science and Technology* 13:75-82.

Waite W.F. et al. 2009. Physical properties of hydrate-bearing soils. *Reviews of Geophysics* 47, RG4003:1-38.